Bioorganic & Medicinal Chemistry 21 (2013) 4332–4341

Contents lists available at SciVerse ScienceDirect

Bioorganic & Medicinal Chemistry

journal homepage: www.elsevier.com/locate/bmc

Exploring DOXP-reductoisomerase binding limits using phosphonated *N*-aryl and *N*-heteroarylcarboxamides as DXR inhibitors

Taryn Bodill [c], Anne C. Conibear [a], Marius K. M. Mutorwa [a], Jessica L. Goble [b], Gregory L. Blatch [b,c,d], Kevin A. Lobb [a,c], Rosalyn Klein [a,c], Perry T. Kaye [a,c,*]

[a] Department of Chemistry, Rhodes University, Grahamstown 6140, South Africa
[b] Biomedical Biotechnology Research Unit and Department of Biochemistry, Rhodes University, Grahamstown 6140, South Africa
[c] Centre for Chemico- and Biomedicinal Research, Rhodes University, Grahamstown 6140, South Africa
[d] College of Health and Biomedicine, Victoria University, Melbourne, Victoria 8001, Australia

ARTICLE INFO

Article history:
Received 13 March 2013
Revised 22 April 2013
Accepted 23 April 2013
Available online 7 May 2013

Keywords:
Anti-malarial
Phosphonates
DOXP-reductoisomerase
Enzyme inhibitors
In silico docking
Saturation transfer difference NMR

ABSTRACT

DOXP-reductoisomerase (DXR) is a validated target for the development of antimalarial drugs to address the increase in resistant strains of *Plasmodium falciparum*. Series of aryl- and heteroarylcarbamoylphosphonic acids, their diethyl esters and disodium salts have been prepared as analogues of the potent DXR inhibitor fosmidomycin. The effects of the carboxamide N-substituents and the length of the methylene linker have been explored using in silico docking studies, saturation transfer difference NMR spectroscopy and enzyme inhibition assays using both *Ec*DXR and *Pf*DXR. These studies indicate an optimal linker length of two methylene units and have confirmed the importance of an additional binding pocket in the *Pf*DXR active site. Insights into the constraints of the *Pf*DXR binding site provide additional scope for the rational design of DXR inhibitors with increased ligand–receptor interactions.

1. Introduction

The *Plasmodium falciparum* enzyme, 1-deoxy-D-xylulose-5-phosphate (DOXP) **1** (Fig. 1) reductoisomerase (*Pf*DXR) is involved in a parasite-specific, isoprenoid biosynthetic DOXP/MEP pathway and has been validated as a target for the design of novel antimalarial drugs.[1,2] Fosmidomycin **2**,[3,4] a natural product isolated from *Streptomyces lavendulae*, and its acetyl analogue, FR900098 **3**,[5,6] have both exhibited DXR-inhibition activity and are important lead compounds in the search for alternative anti-malarial agents. However, absorption, recrudescence and plasma half-life problems[3,5] have precluded the use of fosmidomycin **2** as a drug candidate. The design of potent DXR inhibitors requires an understanding of the essential ligand–enzyme interactions of fosmidomycin as well as the scope for accessing additional binding pockets in the enzyme receptor cavity. Significant features in the design of DXR-inhibiting ligands appear to include the presence of nitrogen- and oxygen-containing functionalities capable of binding the hard Mg^{2+} ion in the DXR active site[7] and replacement of the phosphate group in DOXP **1** by the biologically more stable phosphonate moiety of fosmidomycin **2**.[8,9]

In earlier research on the development of fosmidomycin **2** analogues as potential DXR inhibitors, we have reported: the synthesis and evaluation of *N*-heteroarylamino-2-oxoethylphosphonate esters **5a–e**, the corresponding phosphonic acids **6a–e** and their disodium salts **7a–e** (Scheme 1);[10] and the synthesis of the phosphonated *N*-phenylcarboxamides **5f–l**.[11] In a continuation of these studies, we have been investigating the effects of increasing the length of the linking group between the phosphonate and carboxamide moieties from one to four methylene groups and, in this communication, we now describe: (i) the preparation of the novel 2-(*N*-heteroarylamino)-2-oxoethylphosphonate esters **11a–e**, which contain two methylene groups, their corresponding

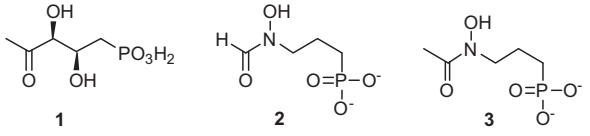

Figure 1. Structures of: the substrate, DOXP **1**; the natural product inhibitor, fosmidomycin **2**; and the synthetic inhibitor, FR900098 **3**.

* Corresponding author. Tel.: +27 46 6038268; fax: +27 46 6225109.
E-mail address: P.Kaye@ru.ac.za (P.T. Kaye).

0968-0896/$ - see front matter © 2013 Elsevier Ltd. All rights reserved.
http://dx.doi.org/10.1016/j.bmc.2013.04.076

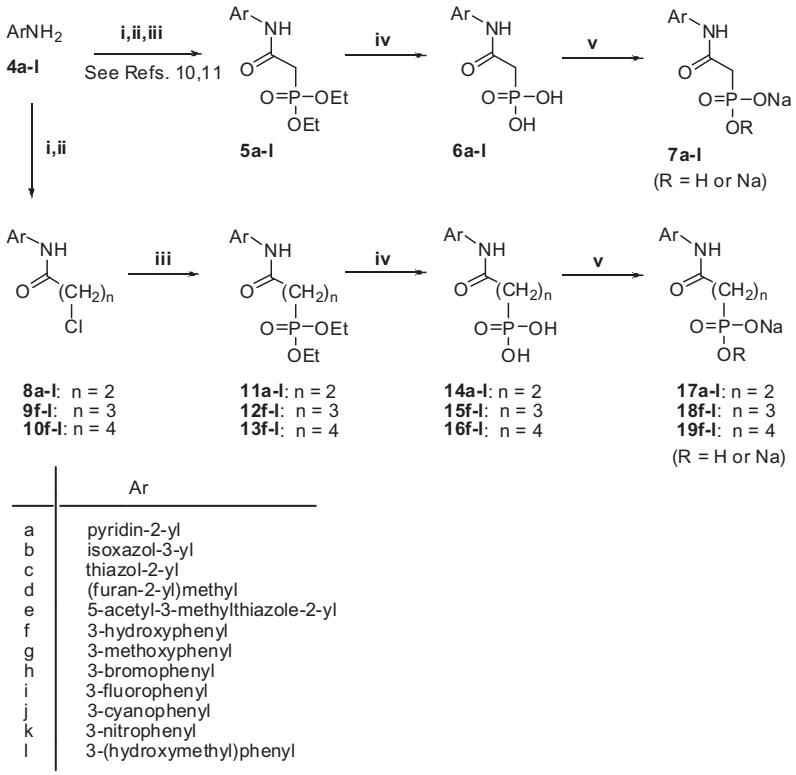

Scheme 1. Synthesis of phosphonate esters, acids and disodium salts. Reagents and conditions: (i) NaH, THF, 6 h, N_2; (ii) $Cl(CH_2)_nCOCl$ (n = 1, 2, 3 or 4), THF, rt; (iii) triethyl phosphite, 9 h, N_2; (iv) TMSBr, DCM, rt, overnight or TMSBr, CH_3CN, 100 °C, 10 min, MeOH/H_2O (95:5 v/v), 30 min, rt; (v) NaOH, EtOH, 30 min, rt.

phosphonic acids **14a–e** and disodium salts **17a–e** (Scheme 1); (ii) the preparation of novel 2-(*N*-arylamino)-2-oxoethylphosphonate esters **11–13f–l**, which contain two, three or four methylene groups, their corresponding phosphonic acids **14–16f–l** and disodium salts **17–19f–l**; and (iii) the results of STD NMR ligand-binding, enzyme inhibition and in silico ligand-docking studies to assess the DXR inhibition potential of selected ligands.

2. Results and discussion

2.1. Chemistry

The phosphonated anilide **5f** (Scheme 1), initially prepared as a truncated ATP analogue,[12] had been found to bind to *Ec*DXR in an STD NMR experiment and to exhibit low-level inhibition of *Ec*DXR. These observations had prompted the synthesis of the aryl- and heteroarylcarbamoylphosphonic acids **6a–l**, their diethyl esters **5a–l** and disodium salts **7a–l** as potential DXR inhibitors, in which the heterocyclic or amide moieties were expected to serve as the metal-chelating group and the phosphonate moiety was expected to occupy its appropriate binding pocket in the enzyme active-site.[10] A three-carbon distance between the phosphonate and hydroxamate moieties is considered essential for the inhibitory activity of fosmidomycin analogues.[13] Consequently, attention was given, in cognate studies,[14,15] to introducing additional methylene groups between the amide and phosphonate moieties.

Thus, the heterocylic amines **4a–e** were deprotonated using sodium hydride and then reacted with 3-chloropropanoyl chloride to afford the dimethylene intermediates **8a–e** (Scheme 1). Similar reactions of the 3-substituted anilines **4f–l** with 3-chloropropanoyl chloride, 4-chlorobutanoyl chloride and 5-chloropentanoyl chloride afforded the corresponding di-, tri- and tetramethylene ω-chloroamides **8–10f–l**. Subsequent Michaelis–Arbuzov reactions[16] between the ω-chloroamides **8a–l**, **9–10f–l** and triethylphosphite under nitrogen yielded the phosphonate esters **11a–l**, and **12–13f–l**. Access to the phosphonic acids **14a–l**, **15–16f–l** was achieved by microwave-assisted[17] or conventional reaction of the phosphonate esters with TMSBr,[10,18] followed by hydrolysis; the corresponding sodium salts were obtained by neutralization with dilute aqueous sodium hydroxide. The final, chromatographed products and their respective precursors were typically obtained in good yields, and all new compounds were fully characterized.

2.2. STD NMR and enzyme-inhibition studies

Selected phosphonate esters and phosphonic acids were subjected to preliminary STD NMR *Ec*DXR enzyme-binding studies and enzyme-inhibition assays using both *Ec*DXR and *Pf*DXR. The phosphonate esters were also evaluated since ester pro-drugs of fosmidomycin analogues have been shown to exhibit increased lipophilicity and absorption.[19–21]

The STD NMR technique, which involves saturation transfer from the enzyme to *bound* ligands, permits the enzyme-binding capacity of a set of ligands to be explored simultaneously.[22] Binding ligands may thus be identified by the presence of corresponding, signals in the STD difference spectrum, as illustrated for compounds **6f**, **14f** and **14g** in Figure 2. STD experiments were conducted on selected phosphonic esters and disodium salts, following the method described by Mayer and Meyer,[22] and the results for the *N*-arylcarboxamides and the *N*-heteroarylcarboxamides are summarized in Tables 1 and 2, respectively. From the STD results, it is apparent that most of the ligands examined bind to the enzyme, notable exceptions being the phosphonic acid salts **16f**, **16h** and **15j**, which failed to exhibit binding. While these results permit rapid, preliminary assessment of binding potential, the possibility of allosteric binding cannot be excluded,[23] and so the enzyme-inhibition potential of selected ligands was also examined using *Ec*DXR and *Pf*DXR.

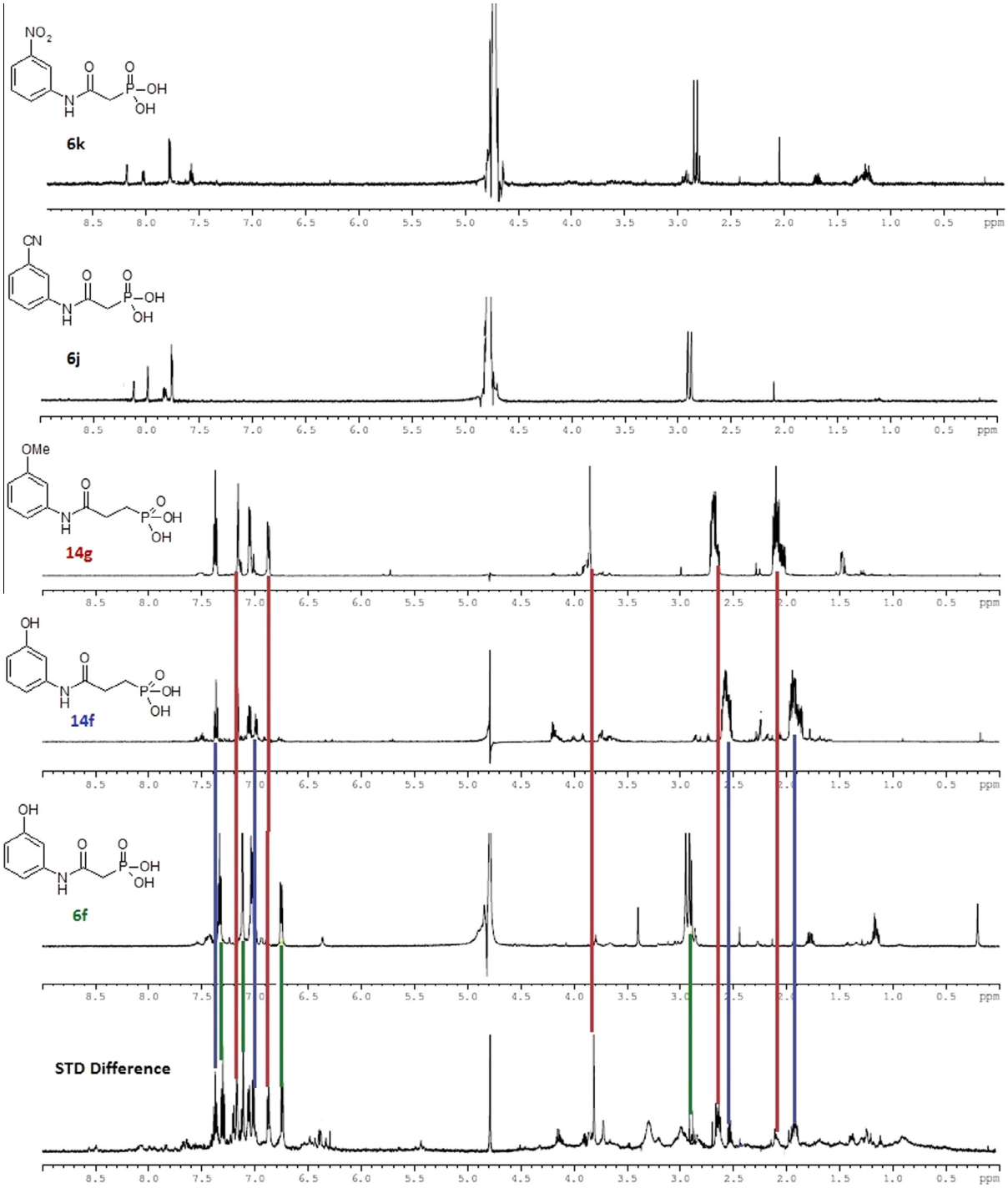

Figure 2. Stack-plot showing results from the *Ec*DXR STD experiment conducted in D_2O with compounds **6f**, **6j**, **14f** and **14g**. The correlations between individual ligand signals and signals in the difference spectrum are indicated by the coloured lines. The absence of STD correlations for ligands **6j** and **6k** indicate that these two ligands failed to bind to the enzyme.

The enzyme-inhibition assays were based on spectrophotometric measurements of the conversion of NADPH to NADP—a reaction concomitant with the DXR-mediated conversion of DOXP to MEP.[9,24,25] Two slightly different assay protocols were followed (Methods A and B as detailed in Section 4). While the bioassays initially focused on the use of readily available *Ec*DXR, the recombinant production of sufficient *Pf*DXR[26] permitted extension of these studies to the latter and clearly more relevant enzyme. The results for the phosphonated *N*-arylcarboxamides (Table 1) reveal that, while the enzyme-inhibition levels are much lower than for fosmidomycin **2** (99.3% inhibition at 0.3 μM), four of the ligands (**5l**, **6f**, **6g** and **6h**) exhibit *Pf*DXR inhibitory activities in excess of 40% at 250 μM. On the other hand, the hydroxylated derivatives **5f**, **5l**, **6g** and **14f** exhibit *Ec*DXR inhibitory activities in excess of 40% at 250 μM (using Method A or Method B). The early observation that increasing the length of the spacer between the phosphonate and carboxamide moieties from one to two methylene groups appeared to enhance *Ec*DXR inhibition activity (cf. **6f** and **14f**; **5f** and **11f**) encouraged us to prepare the series of *N*-heteroarylcarboxamido phosphonate analogues **14a**–**e** with spacers containing

Table 1
STD NMR binding, enzyme-inhibition[a] and in silico active-site docking data for selected phosphonated *N*-arylcarboxamide ligands using recombinant *Ec*DXR at 250 μM

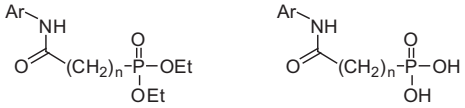

Ar	Compound	*n*	*Ec*DXR inhibition[b] (%)	*Pf*DXR inhibition[c] (%)	Ar	Compound	*n*	*Ec*DXR inhibition[b] (%)	*Pf*DXR inhibition[c] (%)
3-Hydroxyphenyl	**5f**	1	24.4 (44.6)	12.0		**6f**	1	43.9 (34.4)	45.2
	11f	2	33.5 (23.1)	—[d]		**14f**	2 +	49.2 (23.7)	1.1
	12f	3	0.8			**15f**	3 +	0.7	
	13f	4	—[d]			**16f**	4 –	—[d]	
3-Methoxyphenyl	**5g**	1	(11.0)	—[d]		**6g**	1 +	17.8 (31.9)	40.8
	11g	2	14.1 (23.3)	—[d]		**14g**	2 +	—[d] (8.7)	—[d]
	13g	4	—[d]			**16g**	4	—[d]	
3-Bromophenyl	**5h**	1	21.4 (16.3)	—[d]		**6h**	1	26.8 (22.3)	42.0
	12h	3	—[d]			**15h**	2 +	—[d] (32.3)	7.0
3-Cyanophenyl	**5j**	1	11.9 (21.9)	4.8		**16h**	4 –	—[d]	
3-(Hydroxyl-methyl)phenyl	**5l**	1	(40.4)	40.7		**6j**	1	20.0 (8.2)	—[d]
	11l	2	17.9 (17.1)	—[d]		**14l**	2 +	26.8 (16.0)	10.9

[a] Activity in the absence of inhibitor set at 100%, that is 0% inhibition.
[b] Using assay method A; results in parentheses obtained using assay method B.
[c] Using assay method B.
[d] No significant inhibition or anomalous result suggesting enzyme activation.

Table 2
STD NMR binding and enzyme-inhibition data for selected phosphonated *N*-heteroarylcarboxamide ligands using recombinant *Ec*DXR at 500 μM

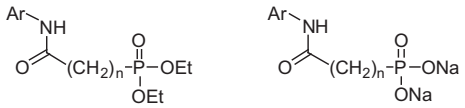

Ar	Compound	*n*	STD result	Enzyme inhibition[a,b] (%)		*n*	STD result	Enzyme inhibition[a,b] (%)
Pyridine-2-yl	**5a**	1	+	58.5[c]	**6a**	1	+	—[c,d]
	11a	2	+	—[c,d]	**14a**	2		0.0
Isoxazoly-3-yl	**5b**	1	+	11.7 [c]	**6b**	1	+	12.2 [c]
	11b	2	+	0.0	**14b**	2	+	0.2
Thiazol-2-yl	**5c**	1	+	28.9 [c]	**6c**	1	+	7.4 [c]
	11c	2	+	0.1	**14c**	2	+	0.2
Furan-2-ylmethyl	**5d**	1	+	67.7 [c]	**6d**	1	+	30.0 [c]
	11d	2	+	0.2	**14d**	2	+	0.3
5-Acetyl-3-methyl-thiazol-2-yl	**5e**	1	+	21.6 [c]	**6e**	1	+	16.6 [c]
	11e	2	+	0.3	**14e**	2	+	0.0

[a] Activity in the absence of inhibitor set at 100%, that is 0% inhibition.
[b] At ligand concentration of 500 μM. At 0.3 μM, fosmidomycin **2** exhibits 99.3% inhibition of *Ec*DXR.
[c] Data from Ref. 10.
[d] Anomalous result suggesting enzyme activation.

two methylene groups. However, although the STD NMR data (Table 2) indicate that these analogues generally bind, in some way, to the enzyme, extension of the spacer beyond one methylene group appears, generally, to decrease inhibition activity. (The data summarised in Table 2 includes, for comparative purposes, results from our earlier study.[10])

Examination of the STD NMR and enzyme-inhibition data summarised in Tables 1 and 2 permits several structure–activity relationship patterns to be identified.

(i) Increasing the number of methylene groups in the spacer (particularly to three or four methylene groups) decreases enzyme-inhibition activity dramatically.
(ii) Generally, in the *N*-arylcarboxamide series, the phosphonic acid salts inhibit *Pf*DXR and *Ec*DXR more effectively than the corresponding phosphonate ester analogues, whereas in the *N*-heteroarylcarboxamide series the pattern is reversed.[10]
(iii) In general, the *Pf*DXR and *Ec*DXR inhibition levels appear to follow similar trends.
(iv) The 3′-oxygenated *N*-arylcarboxamides (3′-OH: **5f**, **6f**, **11f** and **14f**; 3′-CH_2OH: **11l** and **14l**) and the *N*-(furan-2-ylmethyl)carboxamido ligands **5d** and **6d** exhibit the highest enzyme-inhibition levels in their respective series.
(v) The STD binding data do not always correlate with the enzyme-inhibition data, suggesting the possibility of allosteric binding in some cases.
(vi) It might be assumed that the significant decrease in activity, which typically accompanies an increase in the number of methylene units in the spacer between the phosphonate

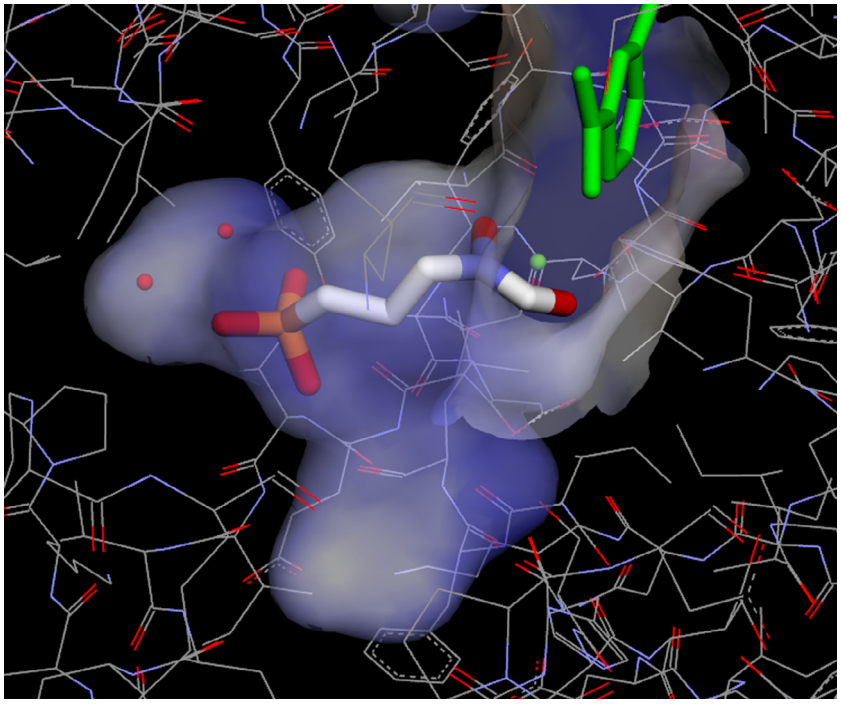

Figure 3. Active site of *Pf*DXR (3AU9[29]), showing the polarity of the cavity around fosmidomycin **2**. The surface zone up to a radius of 7.7 Å from fosmidomycin is shown with 40% transparency and coloured by hydrophobicity [polar (blue), non-polar (white), hydrophobic (orange)]. Protein residues are shown in wireframe, coloured by atom type, fosmidomycin as sticks, coloured by atom type, Mg^{2+} as a pale-green sphere and the crystal structure water molecules as red spheres. NADPH is represented as a green structure.

and metal-binding moieties, simply reflects size constraints in the enzyme binding pockets. However, careful in silico modelling (vide infra) has exposed a deeper complexity.

Selected ligands were also screened for inhibition of *Pf* 3D7 strain growth and for human cell toxicity.[27] Of these, the 3-hydroxymethyl ligand **14l** (R = H) has emerged as a credible lead compound for further research, having been found to: inhibit the action of both the *Pf*DXR and *Ec*DXR enzymes; inhibit the growth of the *P. falciparum* 3D7 strain; and to be non-toxic against the human cell line Hst578T.

2.3. Molecular modelling and simulated docking studies

Deng et al.[28] have reported the synthesis of a series of novel pyridine- and quinoline-containing phosphonate ligands as potential DXR inhibitors, some of which exhibit encouraging activity against *Plasmodium falciparum*. Docking studies of these compounds, which lack the hydroxamate moiety characteristic of fosmidomycin-type ligands, into the receptor cavity of *Ec*DXR, were undertaken by these researchers and, in all cases, the phosphonate groups were found to occupy the phosphate binding site. Interestingly, however, the X-ray crystal structures obtained for three *Ec*DXR–ligand complexes (and used for many of the docking experiments) lacked the Mg^{2+} cation critical for hydroxamate binding.[28] In our study, on the other hand, the ligands all contain amide groups as hydroxamate isosteres and docking studies were undertaken using the recently determined *Pf*DXR crystal structures 3AU9 and 3AUA,[29] which contain bound fosmidomycin **2** and FR900098 **3**, respectively, together with a Mg^{2+} cation and the co-factor NADPH in the active site. The enzymes were prepared for docking studies by removing fosmidomycin **2** or FR900098 **3** and solvating water molecules from the active-sites. We have previously discussed the location of the Mg^{2+} cation in the *Ec*DXR active-site and the importance of assigning a realistic charge to the metal centre;[10] such a charge was used in the present study. Perruchon et al.[9] have highlighted the importance of two negative charges on the ligand, one associated with the metal-coordinating moiety the other with the phosphonate group, and we have found that optimal docking is achieved using models in which two water molecules are associated with the singly deprotonated phosphonate group. As illustrated in Figure 3, fosmidomycin **2** appears to occupy a narrow pocket with the metal ion located at one end near the channel through which the ligand enters, a narrow central region and a phosphonate-binding site in which two water molecules are evident in the crystal structure. The active-site is largely polar (shown in blue), particularly in the vicinity of the metal cation. Closure of the loop region, following binding, results in a relatively confined active-site[30] (Table 3), and variations in the length and characteristics of the three-carbon spacer appear to have been relatively ineffective in increasing enzyme inhibition.[13]

The Accelrys Discovery Studio Visualizer 3.5[31] was used to construct models of the selected compounds in silico as their mono-deprotonated species, both without (*anhydrous*) and with (*hydrated*) two water molecules in close proximity to the phosphonate group. The *hydrated* and *anhydrous* ligands were optimised geometrically and energy-minimised, at the hybrid density functional theory (DFT) B3LYP/3-21G(d) level using GAUSSIAN 03,[32] before being subjected to repeated docking experiments using Autodock Vina version 1.1.1.[33] It was found that docking of the *hydrated* models using Autodock Vina version 1.1.1.[33] located the ligands

Table 3
Dimensions of the active site of the *Pf*DXR (3AU9[29]) crystal structure, with distances measured between specified residues

Dimension	Distance (Å)	Corresponding amino acid residues (atoms)
Length	17.10	Met309 (SD)–Met360 (SD)
Width	15.83	His335 (CD2)–Ile302 (CD1)
Height	9.19	Trp296 (CD1)–Glu315 (CD)

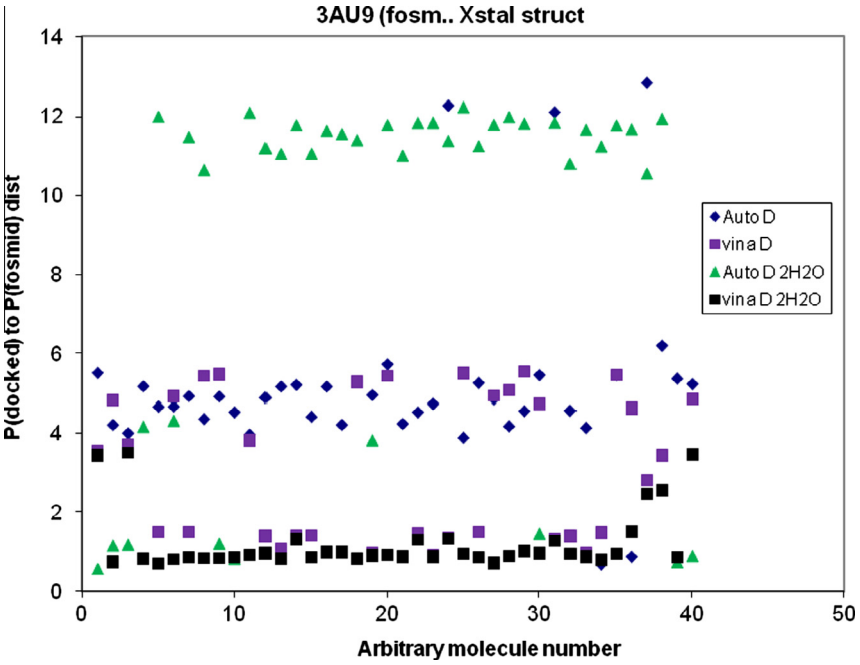

Figure 4. Plots showing variance in the distance (in Å) between the phosphonate phosphorous atoms of ligands [P(docked)] and fosmidomycin **2** [P(fosmid), docked into the active site of *Pf*DXR (3AU9[29]) using:—Autodock version 4.2[34] (AutoD); Autodock Vina version 1.1.1.[33] (vinaD); Autodock version 4.2[34] with hydrated ligands (AutoD $2H_2O$); and Autodock Vina version 1.1.1.[33] with hydrated ligands (vinaD $2H_2O$).

consistently with the phosphonate moiety in close proximity to the crystallographically (3AU9[29]) determined position of the phosphorous atom of fosmidomycin **2**, as shown in Figure 4. (A similar pattern was observed for docking in the analogous system 3AUA.[29]) The data summarized in Figure 4 clearly illustrate the need to evaluate modelling protocols carefully. Docking of '*hydrated*' ligands using Autodock version 4.2[34] typically resulted in significant dislocations (ca. 12 Å) of the phosphonate moiety from the established phosphate binding site, some of which correspond to 'reverse binding' orientations. While docking of '*anhydrous*' ligands using Autodock version 4.2[34] tended to result in smaller dislocations (ca. 5 Å), it is obvious that docking of '*hydrated*' ligands using the more efficient Autodock Vina version 1.1.1.[33] tended, consistently, to locate the phosphonate moiety correctly within the binding site. Given the importance of the phosphonate moiety being negatively charged and having the capacity to engage in hydrogen-bonding

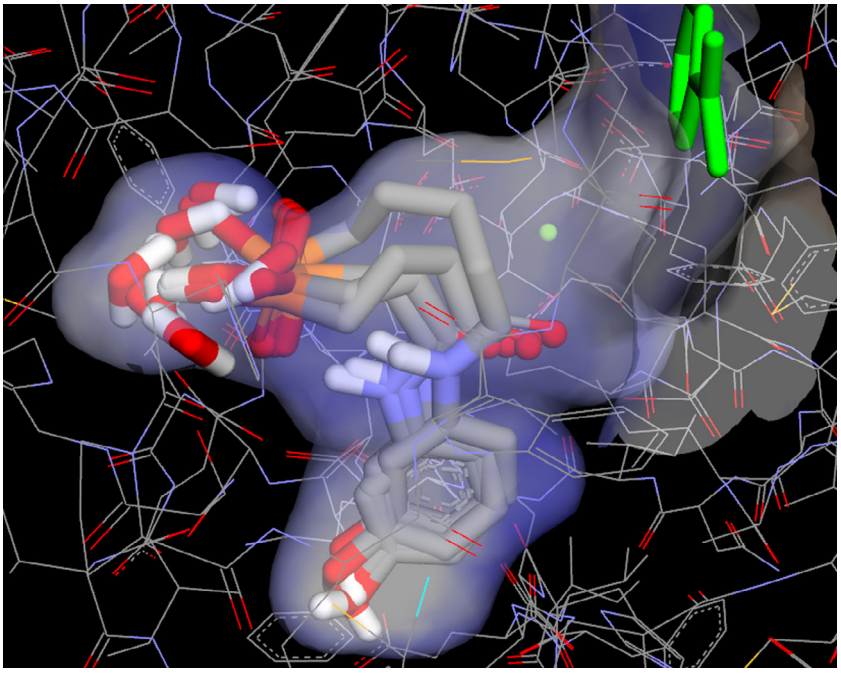

Figure 5. Overlay of ligands **6f**, **14f**, **15f** and **16f** (with the phoshonate moiety hydrated, in each case, with $2 \times H_2O$) docked into the active site of *Pf*DXR (3AU9[29]) using Autodock Vina version 1.1.1.[33] Protein residues are shown in wireframe, coloured by atom type, fosmidomycin as sticks, coloured by atom type, Mg^{2+} as a pale-green sphere. NADPH is represented as a green structure.

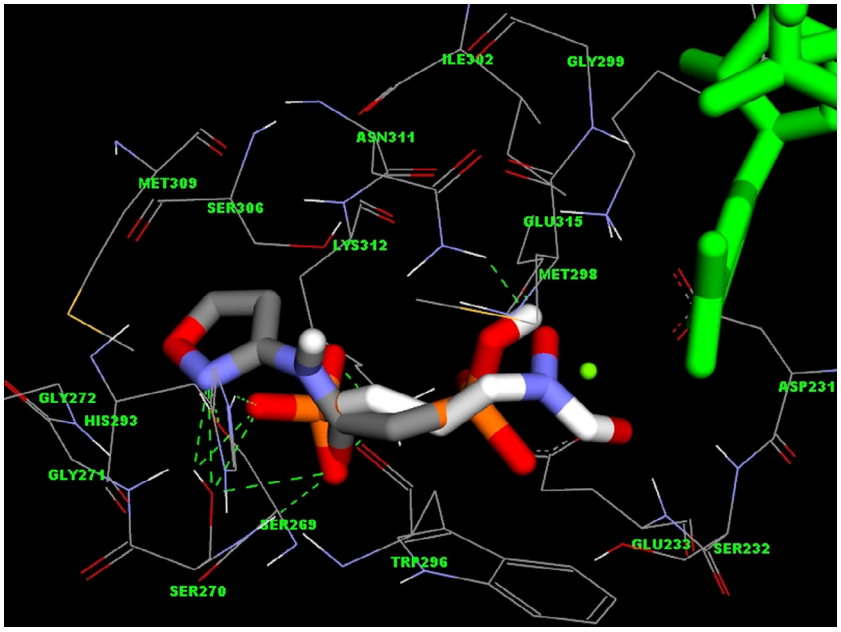

Figure 6. Docked conformation of the isoxazoly-3-yl mono-deprotonated phosphonic acid ligand **6b** in the *Pf*DXR active-site (3AU9),[29] illustrating 'reverse' binding of the ligand relative to fosmidomycin **2**. The crystal structure conformation of fosmidomycin **2** is shown in stick format coloured by atom type (mainly white). Protein active-site residues are shown in wire-frame coloured by atom type, NADPH in stick format coloured green, Mg^{2+} as a green sphere and the ligand shown in stick format coloured by atom type. Some of the hydrogen bonds are shown as green dashed lines. The water molecules have been omitted for clarity.

interactions,[9,35–38] the ligands were docked as their mono-deprotonated phosphonic acid derivatives. The *N*-heteroarylamino phosphonate ester analogues had been shown to be too bulky to fit in the active site[10] and, in any event, were expected to act as pro-drugs, being hydrolyzed in vivo before reaching the active-site.

It was expected that increasing the length of the spacer, linking the metal chelating and phosphonate moieties, would result in the ligand extending beyond the active-site and into the entry channel. Mac Sweeney et al.[39] have suggested that an open conformation of DXR might accommodate larger ligands, while Henriksson et al.[40] have suggested that ligands larger than fosmidomycin **2** might extend into the hydrated cavity, identified in their study of *Mt*DXR. Unexpectedly, however, use of Autodock Vina version 1.1.1.[33] revealed the remarkable tendency of the aromatic moiety in the series of ligands **6f**, **14f**, **15f** and **16f** (n = 1–4) to occupy the available pocket near the metal-chelating site (Fig. 5). The observed decrease in enzyme-inhibition potential (Table 1) may be attributed to the entropic demand associated with the folding required to accommodate the increasing number of internal rotors as the number of methylene groups increases from 1 to 4.

From the STD and enzyme-inhibition data for the phosphonated *N*-arylcarboxamido ligands (Table 1), it is evident that the linking group should contain no more than two methylene groups. Increasing the number of methylene groups in the *N*-heteroarylcarboxamido analogues from one to two, however, clearly precludes efficacious binding (Table 2) and the positive STD data observed for these latter systems is attributed to allosteric binding. It seems that the possibility of ligands occasionally adopting stable docking orientations opposite to that of fosmidomycin **2** cannot be completely excluded. In the case of the isoxazoly-3-yl derivative **6b** (Fig. 6), for example, it might be argued that the mono-deprotonated phosphonate moiety coordinates the Mg^{2+} cation more effectively than the neutral isoxazolyl moiety. Ligands exhibiting such 'reverse' binding may, of course still serve as DXR inhibitors as the binding interactions between the ligands and the enzyme are chemically feasible. In fact, Deng et al.[28] have found 'reversed' in silico EcDXR docking arrangements for both enantiomers of a chiral hydroxamate ligand which exhibits encouraging activity against *Plasmodium falciparum* parasite (EC_{50} of 90 nM). Henriksson et al.[40] and Yajima et al.[41] have reported that the DXR enzyme undergoes conformational changes itself upon binding of a ligand and co-factor, and such changes may permit various plausible orientations of the ligand in the active site.

3. Conclusions

The targeted series of aryl- and heteroarylcarbamoylphosphonic acids, their diethyl esters and disodium salts have been successfully prepared and characterised. Evaluation of selected ligands, using STD NMR, *Pf*DXR and *Ec*DXR enzyme-inhibition and computer-modelling techniques, has provided interesting insights into the importance of receptor-cavity size constraints and the possibilities of allosteric and reverse-orientation ligand binding modes. Future developments are expected to focus on ligands: (i) which contain hydroxyl or furanyl groups; (ii) which contain substituents capable of occupying other pockets in the receptor cavity; and (iii) in which the distance between the phosphonate and metal-binding sites is limited to no more than two methylene groups. On the basis of the results obtained in this study, the 3-hydroxymethyl ligand **14l** (R = H) has emerged as a credible lead compound for further research.

4. Experimental

4.1. Synthesis

The preparation of the aryl- and heteroarylcarbamoylphosphonic acids **6a**–**l**, their diethyl esters **5a**–**l** and disodium salts **7a**–**l** has been reported elsewhere.[10,11] General procedures for the synthesis of the series of compounds **8**–**19** are illustrated by the following examples, while experimental details for the preparation and characterisation of the remaining compounds, most of which are new, are provided in the Supplementary data.

4.1.1. 4-Chloro-*N*-(3-hydroxyphenyl)butanamide 9f

To a stirred solution of 3-aminophenol (1.50 g, 14.0 mmol) in THF (30 mL) under nitrogen was added NaH (60% dispersion in mineral oil; 0.60 g, 24 mmol) in small portions to permit controlled evolution of hydrogen. 4-Chlorobutanoyl chloride (1.18 mL, 14.0 mmol) was then added through a septum and the resulting solution was stirred for ca. 6 h. The solvent was evaporated in vacuo and the residue dissolved in EtOAc (2 × 50 mL). The organic solution was washed sequentially with satd aq $NaHCO_3$ (2 × 100 mL), water (2 × 100 mL) and brine (2 × 100 mL). The aqueous washings were extracted with EtOAc and the combined organic solutions were dried (anhyd $MgSO_4$). Evaporation of the solvent in vacuo afforded 4-chloro-*N*-(3-hydroxyphenyl)butanamide **9f** as a brown solid (2.15 g, 71%) mp 88–90 °C; (found: M^+, 213.05711 $C_{10}H_{12}ClNO_2$ requires: M^+, 213.05566); ν/cm^{-1} 3176 (OH) and 1662 (C=O); δ_H/ppm (400 MHz; $CDCl_3$) 2.17 (2H, m, CH_2CH_2Cl), 2.73 (2H, t, J = 6.8 Hz, CH_2CO), 3.59 (2H, t, J = 6.4 Hz, CH_2Cl), 6.45 (1H, dd, J = 6.0 and 2.0 Hz, 4′-H), 6.51 (1H, dd, J = 6.0 and 2.4 Hz, 6′-H), 6.97 (1H, t, J = 8.0 Hz, 5′-H), 7.48 (1H, t, J = 1.2 Hz, 2′-H), 7.65 (1H, s, OH) and 7.69 (1H, s, NH); δ_C/ppm (100 MHz; $CDCl_3$) 26.8 (CH_2CH_2Cl), 33.1 (CH_2CO), 44.2 (CH_2Cl), 106.4 (C-2′), 109.4 (C-4′), 111.2 (C-6′), 129.7 (C-5′), 139.8 (C-1′), 158.2 (C-3′) and 166.7 (C=O).

4.1.2. Diethyl [*N*-(3-hydroxyphenyl)carbamoyl]ethylphosphonate 11f

Triethyl phosphite (0.86 mL, 5.0 mmol) was added through a septum to 3-chloro-*N*-(3-hydroxyphenyl)propanamide **8f** (0.50 g, 2.5 mmol) under nitrogen in an oven-dried round-bottomed flask equipped with a reflux condenser, and the resulting mixture was refluxed for ca. 9 h during which time the reaction was monitored by TLC. The cooled mixture was then stirred with hexane (20 mL) for ca. 30 min followed by decantation of the hexane layer to remove the excess triethyl phosphite; this was repeated three times. The crude product was purified by flash chromatography [on silica gel; elution with hexane/EtOAc (3:1)], and subsequent evaporation of the solvent in vacuo afforded diethyl [*N*-(3-hydroxyphenyl)carbamoyl]-ethylphosphonate **11f** as a dark brown oil (0.29 g, 58%); (Found: M^+, 301.11247 $C_{13}H_{20}NO_5P$ requires: M^+, 301.10791); ν/cm^{-1} 3261 (OH), 1671 (C=O), 1232 (P=O) and 1024 (P–OEt); δ_H/ppm (400 MHz; $CDCl_3$) 1.29 (6H, t, J = 6.8 Hz, 2 × CH_3), 2.13 (2H, m, CH_2P), 2.68 (2H, m, CH_2CO), 4.06 (4H, m, 2 × OCH_2), 6.60 (1H, d, J = 8.4 Hz, 4′-H), 6.91 (1H, d, J = 7.6 Hz, 6′-H), 7.08 (1H, t, J = 8.0 Hz, 5′-H), 7.36 (1H, s, 2′-H), 8.44 (1H, s, OH) and 8.92 (1H, s, NH); δ_C (100 MHz; $CDCl_3$) 16.2 (d, J_{P-C} = 6.0 Hz, 2 × CH_3), 20.8 (d, J_{P-C} = 142.5 Hz, CH_2P), 27.6 (d, J_{P-C} = 3.7 Hz, CH_2CO), 62.2 (d, J_{P-C} = 6.6 Hz, 2 × OCH_2), 107.2 (C-2′), 111.1 (C-4′), 111.7 (C-6′), 129.4 (C-5′), 139.1 (C-1′), 157.4 (C-3′) and 169.5 (d, J_{P-C} = 15.6 Hz, C=O); δ_P/ppm (162 MHz; $CDCl_3$) 24.1 (P=O).

4.1.3. [*N*-(3-Hydroxyphenyl)carbamoyl]ethylphosphonic acid 14f

Trimethylsilyl bromide (0.22 mL, 1.7 mmol) was added to diethyl [*N*-(3-hydroxyphenyl)carbamoyl]ethyl-phosphonate **11f** (0.25 g, 0.83 mmol) in CH_3CN (3 mL) and the mixture was heated in the microwave apparatus set to deliver 100 W of power, with a reaction temperature of 60 °C and reaction time of 10 min. After completion, the mixture was cooled to room temperature, treated with a 95:5 MeOH/H_2O mixture and stirred for 30 min. The solvent was removed in vacuo and the residue chromatographed [preparative layer chromatography; elution with hexane/EtOAc/MeOH (1:1:1)] to yield [*N*-(3-hydroxyphenyl)carbamoyl]ethylphosphonic acid **14f** as a brown viscous liquid (0.12 g, 61%); (found: C, 44.27; H, 4.98; N, 5.73%. $C_9H_{12}NO_5P$ requires C, 44.09; H, 4.93; N, 5.71%); ν/cm^{-1} 3212 (OH), 1682 (C=O) and 1230 (P=O); δ_H/ppm (400 MHz; DMSO-d_6) 2.12 (2H, m, CH_2P), 2.70 (2H, m, CH_2CO), 5.71 (2H, s, 2 × OH), 6.61 (1H, d, J = 8.2 Hz, 4′-H), 6.89 (1H, d, J = 7.6 Hz, 6′-H), 7.11 (1H, t, J = 8.2 Hz, 5′-H), 7.38 (1H, s, 2′-H), 7.52 (1H, s, OH) and 8.82 (1H, s, NH); δ_C/ppm (100 MHz; DMSO-d_6) 20.7 (d, J_{P-C} = 142.5 Hz, CH_2P), 27.7 (d, J_{P-C} = 3.7 Hz, CH_2CO), 107.1 (C-2′), 111.0 (C-4′), 111.8 (C-6′), 129.8 (C-5′), 139.5 (C-1′), 158.1 (C-3′) and 169.3 (d, J_{P-C} = 15.4 Hz, C=O).

4.1.4. Sodium hydrogen [*N*-(3-hydroxyphenyl)carbamoyl]-ethylphosphonate 17f

[*N*-(3-Hydroxyphenyl)carbamoyl]ethylphosphonic acid **14f** (0.15 g, 0.61 mmol) was treated with a solution of NaOH (1.1 mol) in EtOH (0.58 mL) and the mixture was stirred for 30 min. The solvent was removed in vacuo and the residue chromatographed [reverse-phase column chromatography; elution with H_2O/MeOH (1:1)] to yield sodium hydrogen [*N*-(3-hydroxyphenyl)carbamoyl]ethylphosphonate **17f** as a grey semi-solid (0.12 g, 89%); ν/cm^{-1} 3267 (OH), 1671 (C=O) and 1231 (P=O); δ_H/ppm (400 MHz; D_2O) 2.13 (2H, m, CH_2P), 2.73 (2H, m, CH_2CO), 6.59 (1H, d, J = 8.2 Hz, 4′-H), 6.90 (1H, d, J = 7.6 Hz, 6′-H), 7.12 (1H, t, J = 8.2 Hz, 5′-H) and 7.35 (1H, s, 2′-H); δ_C/ppm (100 MHz; D_2O) 20.6 (d, J_{P-C} = 142.6 Hz, CH_2P), 28.0 (d, J_{P-C} = 3.6 Hz, CH_2CO), 107.2 (C-2′), 110.8 (C-4′), 111.7 (C-6′), 129.5 (C-5′), 139.8 (C-1′), 158.2 (C-3′) and 169.5 (d, J_{P-C} = 15.2 Hz, C=O).

4.2. Saturation transfer difference (STD) experiments

The STD experiments, conducted on a Bruker Avance II* 600 MHz NMR spectrometer, were run for the different sets of ligands as follows: *Ec*DXR, stored in sodium phosphate buffer (pH 7.0), was freeze-dried and re-suspended in D_2O to make a final concentration of 20 μM. Each set of ligands was dissolved in the protein solution to give a final ligand concentration of 800 μM and thus a protein: ligand molar ratio of 1:40. The STD experiment was carried out using parameters optimized in a previous study in our group.[9] The saturating on-resonance and off-resonance pulses were set at frequencies of 0.73 and 20 ppm, respectively, while cycling between the on- and off-resonance phases was used to reduce the effects of changes in temperature or magnetic field homogeneity. A 3-9-19 water suppression pulse was applied at 4.7 ppm and 6000 scans were acquired. The on- and off-resonance spectra were subtracted from each other and processed using Bruker Topspin 2.1 software.

4.3. Expression and purification of *Ec*DXR and *Pf*DXR

*Ec*DXR was expressed and purified according to standard procedures.[25,24] In brief, XL-1 Blue competent cells were transformed with *Ec*DXR plasmid DNA. IPTG was used to induce expression of the recombinant *Ec*DXR gene. The enzyme was then purified by a combination of Ni^{2+} affinity- and size exclusion-chromatography. The protein was stored at −20 °C in a sodium phosphate buffer of pH 7. *Pf*DXR purification was undertaken in a similar manner to that of the *Ec*DXR. However, expression of *Pf*DXR was undertaken using a codon harmonised coding region, under conditions of strongly controlled transcription. This was achieved by heterologous co-expression using the *lac* repressor protein using *Escherichia coli* M15[pREP4] competent cells.[26]

4.4. DXR inhibition assay

As described previously,[10] preliminary screening of the ability of the ligands to inhibit *Ec*DXR and *Pf*DXR was conducted using an enzyme assay based on the spectrophotometric measurement of the conversion of NADPH to NADP which occurs when DOXP **1** is converted to MEP by DXR.

Method A: Assays were conducted in a reaction mixture containing 100 mM Tris–HCl (pH 7.5), 1 mM $MgCl_2$, 0.3 mM NADPH and 0.3 mM DOXP in a total volume of 100 μL. Equal volumes of *Ec*DXR and ligand were pre-incubated at 37 °C for 5 min; 100 μL of this enzyme–ligand mixture was then added to the rest of the assay components to make a total of 200 μL with a final *Ec*DXR concentration of 5 μg/mL. The decrease in absorbance at 340 nm due to the decreasing concentration of NADPH ($\varepsilon_{NADPH} = 6.3 \times 10^3$ L mol^{-1} cm^{-1}) was followed for 10 min at 37 °C, relative to a blank lacking the DOXP substrate. For each ligand, enzyme activity in the absence of inhibitor was deemed to be 100% (i.e., 0% inhibition) and the % relative inhibition was determined in triplicate. The ligands were tested at concentrations between 10 μM and 500 μM, and the 250 or 500 μM data (Tables 1 and 2, respectively) were used to assess their inhibition potential. Since fosmidomycin **2** is a slow, tight-binding inhibitor of DXR,[42] the synthesized ligands were pre-incubated with the enzyme and NADPH before the reaction was initiated with the addition of the substrate, DOXP **1**. For each ligand, the bioassays were carried out in triplicate and the specific activity of the enzyme was determined by analyzing the linear portion of the graph generated by plotting average absorbance (at 340 nm) against time (over 10 min). The specific activity of the enzyme in the experiment lacking a ligand was considered to be 100% (i.e., 0% inhibition), which allowed the inhibitory activities to be expressed as relative percentages. Fosmidomycin **2** was used as a positive control for DXR inhibition and exhibited 99.3% inhibition at 0.3 μM.

Method B:[27] Assays were performed in a reaction mixture containing 100 mM Tris–HCl (pH 7.5), 1 mM $MnCl_2$, 0.3 mM NADPH, 0.3 mM DOXP substrate[6] and DXR (5–20 μg/mL), made a final volume of 200 μL with assay buffer. Samples were incubated at 37 °C for 5 min before the reaction was initiated by adding 20 μg/mL purified *Pf*DXR or 5 μg/mL purified *Ec*DXR. The oxidation of NADPH was monitored at 340 nm using a PowerWave™ microtitre plate reader, using a flat-bottomed 96-well microtitre plate, adjusted to 37 °C. Reactions were blanked against a reaction containing water with 2% DMSO (no enzyme). Activity of DXR was expressed in units per mg of protein where 1 unit is defined as the amount of enzyme that causes oxidation of 1 μmol of NADPH per minute; the extinction coefficient for NADPH used in this work was 6.3×10^3 L mol^{-1} cm^{-1} at 340 nm. Control reactions that were incorporated prior to assay analysis included: no enzyme; denatured enzyme (boiled); no NADPH; and no divalent ion.

4.5. Molecular modelling and simulated docking studies

The Accelrys Discovery Studio Visualizer 3.5[31] was used to construct the selected compounds in silico as their mono-deprotonated species, both with (hydrated) and without (anhydrous) two water molecules in proximity to the phosphonate group. Using GAUSSIAN 03,[32] the structure for each compound was optimised geometrically and energy-minimised at the hybrid density functional theory (DFT) B3LYP/3-21G(d) level. Docking studies of the geometry optimised and energy-minimised hydrated and anhydrous ligands was carried out using Autodock version 4.2[34] and Autodock Vina version 1.1.1.[33] separately, using the crystallographically-determined *Pf*DXR enzyme structures, 3AU9 and 3AUA,[29] as the protein-receptor models, while the docked conformations were visualized using the Accelrys Discovery Studio Visualizer 3.5[31] The X-ray crystal structure *Pf*DXR 3AU9 is complexed with fosmidomycin 2, while *Pf*DXR 3AUA is complexed with FR900098 3;[29] both structures contain the divalent metal cation Mg^{2+} and the NADPH co-factor.

To validate the reliability of the docking procedure, fosmidomycin **2** and FR900098 **3** were removed from the receptor cavities of the respective proteins, energy-minimised (as anhydrous and hydrated structures) and re-docked into the protein. Simulated docking of the energy minimised ligands involved the removal of fosmidomycin **2** (or FR900098 3) and the solvating water molecules from the active sites of the *Pf*DXR crystal structures (3AU9 and 3AUA),[29] whilst the NADPH co-factor was retained. Using Autodock Tools, Gasteiger charges were added and non-polar hydrogens were merged for the respective ligands and the protein model, while the active-site residues Ser270, Ser306, Asn311, Lys312 and Glu315 were assigned as flexible.

Docking using AutoDock 4.2[34] involved the initial use of the AutoGrid 4.2 algorithm to represent the active site with a grid box of dimensions $70 \times 70 \times 65$ units (grid-point spacing of 0.375 Å) along the *x*-, *y*- and *z*-directions centered on the original fosmidomycin **2** or FR900098 **3** ligand position, and atom maps were calculated for all possible active-site residue-ligand interactions. In silico dockings were conducted using the Lamarckian algorithm with a population size of 150, allowing for a maximum of 27,000 generations and 4.5×10^6 energy evaluations. For each ligand docking experiment, 100 possible docked-conformers were generated. Autodock Vina[33] was also used to dock the anhydrous and hydrated ligands to the *Pf* DXR structures (3AU9 and 3AUA[29]). The proteins and ligands were prepared as for the AutoDock 4.2 experiments, and the same flexible residues were specified. The dimension of the search area was 11 Å, and the exhaustiveness was set to a value of 64.

The best docked-conformer for each of the ligands was selected upon analysis of: (i) the ligand binding affinity;[36,37] (ii) the position of the ligand P atom relative to the ligand P in the crystal structures and; (iii) the ligand efficiency[43,44] relative to fosmidomycin. The ligand efficiency is a measure of the binding free energy per atom of the ligand and provides an indication of the quality of fit of the ligand within the active site of the enzyme. A ligand is classified as having a good binding affinity and good ligand efficiency by the magnitude of the negative values; hydrated fosmidomycin **2** exhibited a binding affinity of −8 kcal mol^{-1} when re-docked to 3AU9[29] using AutoDock Vina.[33]

Acknowledgments

The authors thank the Beit Trust for a bursary (to A.C.C.), Rhodes University, LIFE*lab* and the South African Medical Research Council (MRC) for generous financial support, Professor Hassan Jomaa (Institute of Biochemistry, Academic Hospital Centre, Justus-Liebig University) for the gift of the DXR plasmid and referees for helpful comments.

Supplementary data

Supplementary data associated with this article can be found, in the online version, at http://dx.doi.org/10.1016/j.bmc.2013.04.076.

References and notes

1. Rohmer, M.; Seemann, M.; Horbach, S.; Bringer-Meyer, S.; Sahm, H. *J. Am. Chem. Soc.* **1996**, *118*, 2564.
2. Lichtenthaler, H. K. *Biochem. Soc. Trans.* **2000**, *28*, 785.
3. Wiesner, J.; Borrmann, S.; Jomaa, H. *Parasitol. Res.* **2003**, *90*, S71.
4. Okuhara, M.; Kuroda, Y.; Goto, T. *J. Antibiot.* **1980**, *33*, 13.
5. Singh, N.; Cheve, G.; Avery, M. A.; McCurdy, C. R. *Curr. Pharm. Des.* **2007**, *13*, 1161.
6. Jomaa, H.; Wiesner, J.; Sanderbrand, S.; Altincicek, B.; Weidemeyer, C.; Hintz, M.; Türbachova, I.; Eberl, M.; Zeidler, J.; Lichtenthaler, H. K.; Soldati, D.; Beck, E. *Science* **1999**, *285*, 1573.
7. Deng, L.; Sundriyal, S.; Rubio, V.; Shi, Z. Z.; Song, Y. *J. Med. Chem.* **2009**, *52*, 6539.
8. Meyer, O.; Grosdemange-Billiard, C.; Tritsch, D.; Rohmer, M. *Org. Biomol. Chem.* **2003**, *1*, 4367.
9. Perruchon, J.; Ortmann, R.; Altenkämper, M.; Silber, K.; Wiesner, J.; Jomaa, H.; Klebe, G.; Schlitzer, M. *ChemMedChem* **2008**, *3*, 1232.
10. Bodill, T.; Conibear, A. C.; Blatch, G. L.; Lobb, K. A.; Kaye, P. T. *Bioorg. Med. Chem.* **2011**, *19*, 1321.

11. Mutorwa, M.; Salisu, S.; Blatch, G. L.; Kenyon, C.; Kaye, P. T. *Synth. Commun.* **2009**, *39*, 2723.
12. Salisu, S. T. ATP Mimics as Glutamine Synthetase Inhibitors - An Exploratory Study. PhD Thesis, Rhodes University, 2008.
13. Hemmi, K.; Takeno, H.; Hashimoto, M.; Kamiya, T. *Chem. Pharm. Bull.* **1982**, *30*, 111.
14. Conibear, A. C. Synthesis and Evaluation of Novel Inhibitors of 1-Deoxy-D-xylulose-5-phosphate Reductoisomerase as Potential Antimalarials. M.Sc. Thesis, Rhodes University, 2010.
15. Mutorwa, M. K. M. Synthesis of Novel Inhibitors of 1-deoxy-D-xylulose-5-phosphate Reductoisomerase as Potential Anti-malarial Lead Compounds. Ph.D. Thesis, Rhodes University, 2011.
16. Bhattacharya, A. K.; Thyagarajan, G. *Chem. Rev.* **1981**, *81*, 415.
17. Kumar, K. G. D.; Saenz, D.; Lokesh, G. L.; Natarajan, A. *Tetrahedron Lett.* **2006**, *47*, 6281.
18. McKenna, C. E.; Higa, M. T.; Cheung, N. H.; McKenna, M. *Tetrahedron Lett.* **1977**, *18*, 155.
19. Ortmann, R.; Wiesner, J.; Reichenberg, A.; Henschker, D.; Beck, E.; Jomaa, H.; Schlitzer, M. *Bioorg. Med. Chem. Lett.* **2003**, *13*, 2163.
20. Reichenberg, A.; Wiesner, J.; Weidemeyer, C.; Dreiseidler, E.; Sanderbrand, S.; Altincicek, B.; Beck, E.; Schlitzer, M.; Jomaa, H. *Bioorg. Med. Chem. Lett.* **2001**, *11*, 833.
21. Kurz, T.; Schlüter, K.; Kaula, U.; Bergmann, B.; WalterGeffken, D, R. D.; Geffken, D. *Bioorg. Med. Chem.* **2006**, *14*, 5121.
22. Mayer, M.; Meyer, B. *Angew. Chem., Int. Ed.* **1999**, *38*, 1784.
23. Ji, Z.; Yao, Z.; Liu, M. *Anal. Biochem.* **2009**, *385*, 380.
24. Kuzuyama, T.; Shimizu, T.; Takahashi, S.; Seto, H. *Tetrahedron Lett.* **1998**, *39*, 7913.
25. Kuntz, L.; Tritsch, D.; Grosdemange-Billiard, C.; Hemmerlin, A.; Willem, A.; Bach, T. J.; Rohmer, M. *Biochem. J.* **2005**, *386*, 127.
26. Goble, J. L.; Johnson, H.; de Ridder, J.; Stephens, L. L.; Louw, A.; Blatch, G. L.; Boshoff, A. *Protein Pept. Lett.* **2013**, *20*, 115.
27. Goble, J. L. The Druggable Anti-malarial Target 1-Deoxy-D-xylulose-5-phosphate Reductoisomerase: Purification, Kinetic Characterisation and Inhibition Studies. Ph.D. Thesis, Rhodes University, Grahamstown, 2011.
28. Deng, L.; Endo, K.; Kato, M.; Cheng, G.; Yajima, S.; Song, Y. *ACS Med. Chem. Lett.* **2011**, *2*, 165.
29. Umeda, T.; Tanaka, N.; Kusakabe, Y.; Nakanishsi, M.; Kitade, Y.; Nakamura, K. T. *Sci. Rep.* **2011**, *1*, 1.
30. Pettersen, E. F.; Goddard, T. D.; Huang, C. C.; Couch, G. S.; Greenblatt, D. M.; Meng, E. C.; Ferrin, T. E. *J. Comput. Chem.* **2004**, *25*, 1605.
31. Discovery Studio Modeling Environment, Release 3.5, Accelrys Software Inc.: San Diego, 2012.
32. Frisch, M. J.; Trucks, G. W.; Schlegel, H. B.; Scuseria, G. E.; Robb, M. A.; Cheeseman, J. R.; Montgomery, J. A., Jr.; Vreven, T.; Kudin, K. N.; Burant, J. C.; Millam, J. M.; Iyengar, S. S.; Tomasi, J.; Barone, V.; Mennucci, B.; Cossi, M.; Scalmani, G.; Rega, N.; Petersson, G. A.; Nakatsuji, H.; Hada, M.; Ehara, M.; Toyota, K.; Fukuda, R.; Hasegawa, J.; Ishida, M.; Nakajima, T.; Honda, Y.; Kitao, O.; Nakai, H.; Klene, M.; Li, X.; Knox, J. E.; Hratchian, H. P.; Cross, J. B.; Bakken, V.; Adamo, C.; Jaramillo, J.; Gomperts, R.; Stratmann, R. E.; Yazyev, O.; Austin, A. J.; Cammi, R.; Pomelli, C.; Ochterski, J. W.; Ayala, P. Y.; Morokuma, K.; Voth, G. A.; Salvador, P.; Dannenberg, J. J.; Zakrzewski, V. G.; Dapprich, S.; Daniels, A. D.; Strain, M. C.; Farkas, O.; Malick, D. K.; Rabuck, A. D.; Raghavachari, K.; Foresman, J. B.; Ortiz, J. V.; Cui, Q.; Baboul, A. G.; Clifford, S.; Cioslowski, J.; Stefanov, B. B.; Liu, G.; Liashenko, A.; Piskorz, P.; Komaromi, I.; Martin, R. L.; Fox, D. J.; Keith, T.; Al-Laham, M. A.; Peng, C. Y.; Nanayakkara, A.; Challacombe, M.; Gill, P. M. W.; Johnson, B.; Chen, W.; Wong, M. W.; Gonzalez, C.; Pople, J. A. GAUSSIAN *03, Revision E.01*; Gaussian: Wallingford, CT, 2004.
33. Trott, O.; Olsen, A. J. *J. Comput. Chem.* **2010**, *31*, 455.
34. Morris, G. M.; Goodsell, D. S.; Halliday, R. S.; Huey, R.; Hart, W. E.; Belew, R. K.; Olson, A. J. *J. Comput. Chem.* **1998**, *19*, 1639.
35. Silber, K.; Heidler, P.; Kurz, T.; Klebe, G. *J. Med. Chem.* **2005**, *48*, 3547.
36. Tao, P.; Lai, L. *J. Comput. Aided Mol. Des.* **2001**, *15*, 429.
37. Kim, R.; Skolnick, J. *J. Comput. Chem.* **2008**, *29*, 1316.
38. Giessmann, D.; Heidler, P.; Haemers, T.; Van Calenbergh, S.; Reichenberg, A.; Jomaa, H.; Weidemeyer, C.; Sanderbrand, S.; Wiesner, J.; Link, A. *Chem. Biodivers.* **2008**, *5*, 643.
39. Mac Sweeney, A.; Lange, R.; Fernandes, R. P. M.; Schulz, H.; Dale, G. E.; Douangamath, A.; Proteau, P. J.; Oefner, C. *J. Mol. Biol.* **2005**, *345*, 115.
40. Henriksson, L. M.; Unge, T.; Carlsson, J.; Aqvist, J.; Mowbray, S. L.; Jones, T. A. *J. Biol. Chem.* **2007**, *282*, 19905.
41. Yajima, S.; Nonaka, T.; Kuzuyama, T.; Seto, H.; Ohsawa, K. *J. Biochem.* **2002**, *131*, 313.
42. Koppisch, A. T.; Fox, D. T.; Blagg, B. S. J.; Poulter, C. D. *Biochemistry (N.Y.)* **2002**, *41*, 236.
43. Reynolds, C. H.; Tounge, B. A.; Bembenek, S. D. *J. Med. Chem.* **2008**, *51*, 2432.
44. Reynolds, C. H.; Tounge, B. A.; Bembenek, S. D. *Drug Discovery Today* **2009**, *14*, 278.